Acta Crystallographica Section B
Structural Science
ISSN 0108-7681

Quantitative analysis of hydrogen bonding and atomic thermal motion in the organic non-linear optical material DCNP using X-ray and neutron diffraction

Jacqueline M. Cole,[a]*† Chick C. Wilson,[b] Judith A. K. Howard[c] and Frank R. Cruickshank[d]

[a]Institut Laue–Langevin, BP 156, 38042 Grenoble CEDEX 9, France, [b]The ISIS Facility, Rutherford Appleton Laboratory, Chilton, Didcot, Oxon OX11 0QX, England, [c]Chemistry Department, University of Durham, South Road, Durham DH1 3LE, England, and [d]Department of Pure and Applied Chemistry, University of Strathclyde, 295 Cathedral Street, Glasgow G1 1XL, Scotland

† Present address: Department of Chemistry, University of Cambridge, Lensfield Road, Cambridge CB2 1EW, England.

Correspondence e-mail: jmc61@cam.ac.uk

Received 24 November 1999
Accepted 22 June 2000

A single-crystal neutron diffraction study of the organic non-linear optical material 3-(1,1-dicyanoethenyl)-1-phenyl-4,5-dihydro-1*H*-pyrazole (hereafter DCNP), space group *Cc*, is presented. The study was conducted in order to relate the structural characteristics of the compound to its physical properties. DCNP exhibits a very large second harmonic generation (SHG) output, an extremely large linear electro-optical effect and photoconductive and pyroelectric properties. The nature of the hydrogen-bonding revealed by the study, in part, accounts for the first two of these phenomena. The neutron study also shows that some rather atypical atomic thermal motion is present in part of the molecule. With the aid of a variable-temperature single-crystal X-ray diffraction study, in conjunction with the neutron study, this thermal motion is attributed to libration and is fully characterized. As a result, suitable corrections to the bond geometry and the anisotropic displacement parameters of DCNP are made. The libration is also shown to enhance the SHG effect. The cell parameters from the variable-temperature X-ray study are also used in order to evaluate the thermal expansivity coefficients of DCNP.

1. Introduction

Recent advances in organic non-linear optical (NLO) materials have invoked a large revival of interest in this area of research on account of their widespread industrial potential. In particular, studies have concentrated on second harmonic generation (SHG), the first-order NLO effect. Results have shown that an inherent relationship exists between the structure of these materials and their observed properties. On the molecular scale, the extent of charge transfer is assumed to dominate the SHG output (Davydov *et al.*, 1970; Oudar & Zyss, 1982; Oudar, 1977; Lalama & Garito, 1979; Albrecht & Morell, 1979), whilst on the supramolecular scale, a high SHG output requires non-centrosymmetry (Cady, 1946), strong intermolecular interactions (Sarma *et al.*, 1997; Cole, 1997; Ravi *et al.*, 1998) and good phase-matching ability (Franken & Ward, 1963; Giordmaine, 1962; Maker *et al.*, 1962).

The presence of an aromatic ring was one of the first structural features to be recognized as an important constituent of an SHG active material (Davydov *et al.*, 1970). The reason for its importance is twofold: firstly, it is often the π–π^* aromatic electronic transition which is responsible for the SHG effect; secondly, the extended conjugation present in such a ring aids charge transfer to propagate across the ring through vicinal conjugated branches of atoms. However, it was later recognized that the ring current created by the aromatic delocalization of electrons is an unfavourable feature, since it

Table 1
Experimental details.

	100 K (neutron)	90 K (X-ray)	100 K (X-ray)	200 K (X-ray)	290 K (X-ray)
Crystal data					
Chemical formula	$C_{13}H_{10}N_4$	$C_{13}H_{10}N_4$	$C_{13}H_{10}N_4$	$C_{13}H_{10}N_4$	$C_{13}H_{10}N_4$
Chemical formula weight	222	222.25	222.25	222.25	222.25
Cell setting	Monoclinic	Monoclinic	Monoclinic	Monoclinic	Monoclinic
Space group	*Cc*	*Cc*	*Cc*	*Cc*	*Cc*
a (Å)	11.571 (2)	11.5945 (3)	11.5972 (2)	11.7304 (4)	11.8751 (5)
b (Å)	12.258 (3)	12.2912 (4)	12.2873 (2)	12.3278 (2)	12.3735 (5)
c (Å)	7.868 (2)	7.8944 (2)	7.8877 (1)	7.8844 (2)	7.8876 (3)
β (°)	90.11 (3)	90.018 (1)	90.021 (1)	90.173 (2)	90.412 (2)
V (Å^3)	1116.0 (4)	1125.03 (3)	1123.98 (3)	1140.16 (5)	1158.95 (8)
Z	4	4	4	4	4
D_x (Mg m^{-3})	1.321	1.312	1.313	1.295	1.274
Radiation type	Pulsed neutrons at ISIS, UK	Mo $K\alpha$	Mo $K\alpha$	Mo $K\alpha$	Mo $K\alpha$
Wavelength (Å)	Variable (time-of-flight)	0.71073	0.71073	0.71073	0.71073
μ (mm^{-1})	Variable (time-of-flight)	0.083	0.083	0.082	0.081
Temperature (K)	100 (2)	90 (2)	100 (2)	200 (2)	290 (2)
Crystal form	Pointed needle	Irregular	Irregular	Irregular	Irregular
Crystal size (mm)	7.0 × 3.0 × 2.0	0.5 × 0.3 × 0.15	0.5 × 0.3 × 0.15	0.5 × 0.3 × 0.15	0.5 × 0.3 × 0.15
Crystal colour	Red	Red	Red	Red	Red
Data collection					
Diffractometer	SXD at ISIS, UK	Siemens SMART-CCD	Siemens SMART-CCD	Siemens SMART-CCD	Siemens SMART-CCD
Data collection method	Laue diffraction scans	ω scans	ω scans	ω scans	ω scans
Absorption correction	Semi-empirical (Wilson, 1997)	None	None	None	None
No. of measured reflections	7808	3921	16 798	4054	4000
No. of independent reflections (including Friedel pairs)	1867	2029	10 048	2402	2112
No. of observed reflections	1863	1893	6421	2394	1557
Criterion for observed reflections	$I > 2\sigma(I)$	$I > 2\sigma(I)$	$I > 2\sigma(I)$	$I > 2\sigma(I)$	$I > 2\sigma(I)$
R_{int}	0.060	0.0300	0.0288	0.0377	0.0346
$(\sin\theta/\lambda)_{max}$ (Å^{-1})	0.8	0.65	1.13	0.65	0.65
Range of h, k, l	$0 \rightarrow h \rightarrow 34$ $0 \rightarrow k \rightarrow 38$ $-27 \rightarrow l \rightarrow 23$	$-14 \rightarrow h \rightarrow 15$ $-12 \rightarrow k \rightarrow 15$ $-10 \rightarrow l \rightarrow 10$	$-26 \rightarrow h \rightarrow 25$ $-27 \rightarrow k \rightarrow 23$ $-17 \rightarrow l \rightarrow 16$	$-15 \rightarrow h \rightarrow 15$ $-11 \rightarrow k \rightarrow 16$ $-9 \rightarrow l \rightarrow 10$	$-14 \rightarrow h \rightarrow 15$ $-13 \rightarrow k \rightarrow 16$ $-10 \rightarrow l \rightarrow 10$
Refinement					
Refinement on	F^2	F^2	F^2	F^2	F^2
$R[F^2>2\sigma(F^2)]$	0.0731	0.0348	0.0763	0.0463	0.0514
$wR(F^2)$	0.0832	0.0787	0.0745	0.0678	0.0886
S	4.016	1.117	2.846	1.721	1.297
No. of reflections used in refinement	1863	2028	9977	2394	2098
No. of parameters used	244	195	194	195	195
H-atom treatment	All parameters refined	xyz and U_{iso} refined	xyz and U_{iso} refined	xyz and U_{iso} refined	xyz and U_{iso} refined
Weighting scheme	$w = 1/[\sigma^2(F_o^2)]$, where $P = (F_o^2 + 2F_c^2)/3$	$w = 1/[\sigma^2(F_o^2) + (0.0274P)^2 + 0.5936P]$, where $P = (F_o^2 + 2F_c^2)/3$	$w = 1/[\sigma^2(F_o^2)$, where $P = (F_o^2 + 2F_c^2)/3$	$w = 1/[\sigma^2(F_o^2)]$, where $P = (F_o^2 + 2F_c^2)/3$	$w = 1/[\sigma^2(F_o^2) + (0.0130P)^2 + 0.3922P]$, where $P = (F_o^2 + 2F_c^2)/3$
$(\Delta/\sigma)_{max}$	0.024	<0.001	0.003	0.001	<0.001
$\Delta\rho_{max}$ (e Å^{-3} or fm Å^{-3})	2.224	0.152	0.765	0.221	0.111
$\Delta\rho_{min}$ (e Å^{-3} or fm Å^{-3})	−1.463	−0.155	−0.441	−0.147	−0.099
Extinction method	None	*SHELXL*	None	*SHELXL*	*SHELXL*
Extinction coefficient	–	0.0045 (7)	–	0.020 (2)	0.0116 (10)
Source of atomic scattering factors	*International Tables for Crystallography* (1992, Vol. C, Table 4.4.4.1)	*International Tables for Crystallography* (1992, Vol. C, Tables 4.2.6.8 and 6.1.1.4)	*International Tables for Crystallography* (1992, Vol. C, Tables 4.2.6.8 and 6.1.1.4)	*International Tables for Crystallography* (1992, Vol. C, Tables 4.2.6.8 and 6.1.1.4)	*International Tables for Crystallography* (1992, Vol. C, Tables 4.2.6.8 and 6.1.1.4)
Computer programs					
Data collection	Local *ISIS* program	*SMART* (Siemens, 1995)	*SMART* (Siemens, 1995)	*SMART* (Siemens, 1995)	*SMART* (Siemens, 1995)
Cell refinement	Local *ISIS* program	*SMART* (Siemens, 1995)	*SMART* (Siemens, 1995)	*SMART* (Siemens, 1995)	*SMART* (Siemens, 1995)
Data reduction	Local *ISIS* program	*SMART* (Siemens, 1995)	*SMART* (Siemens, 1995)	*SMART* (Siemens, 1995)	*SMART* (Siemens, 1995)
Structure solution	None	*SHELXS*86 (Sheldrick, 1990)	*SHELXS*86 (Sheldrick, 1990)	*SHELXS*86 (Sheldrick, 1990)	*SHELXS*86 (Sheldrick, 1990)

Table 1 (continued)

	100 K (neutron)	90 K (X-ray)	100 K (X-ray)	200 K (X-ray)	290 K (X-ray)
Structure refinement	*SHELXL*93 (Sheldrick, 1993)	*SHELXL*93 (Sheldrick, 1993)	*SHELXL*93 (Sheldrick, 1993)	*SHELXL*93 (Sheldrick, 1993)	*SHELXL*93 (Sheldrick, 1993)
Preparation of material for publication	*SHELXL*93 (Sheldrick, 1993)	*SHELXL*93 (Sheldrick, 1993)	*SHELXL*93 (Sheldrick, 1993)	*SHELXL*93 (Sheldrick, 1993)	*SHELXL*93 (Sheldrick, 1993)

makes the necessary polarization of a phenyl unit into a quinoidal form energetically costly (Brédas & Street, 1985). This leads to a localization of donor and acceptor interactions and a hampering of extended charge transfer across a molecule. Indeed, if the delocalization energy in such a ring is reduced (i) by substitution of a heteroatomic atom such as sulfur or nitrogen, (ii) by changing the size of the ring or (iii) by removing the full level of conguation in the ring, the charge transfer is ameliorated (for example, Jen *et al.*, 1993; Cheng *et al.*, 1991). Of these 'reduced' aromatic rings, the pyrazole ring showed particularly high potential and promising results were obtained from calculations (Docherty *et al.*, 1985) of dipole moments and molecular hyperpolarizabilities (both static and dynamic) for six 1,3-disubstituents. Subsequent experimental work (Allen *et al.*, 1988) on a series of 1,3-disubstituted 4,5-dihydro-1*H*-pyrazoles was conducted in order to assess the materials for linear optical, linear electro-optical and NLO potential. The subject compound, 3-(1,1-dicyanoethenyl)-1-phenyl-4,5-dihydro-1*H*-pyrazole (hereafter DCNP), was the most promising of the compounds in this reported study. With further work (Miniewicz *et al.*, 1994; Allen *et al.*, 1988; Black *et al.*, 1993) it was revealed that DCNP showed exceptional NLO potential, giving powder SHG signals of approximately 100 times that of urea when using a fundamental wavelength, λ_f, of 1.9 μm. At the more common $\lambda_f = 1.06$ μm, a signal of only 1.6 times that of urea resulted, but this is simply because of the re-absorption of the 532 nm harmonic radiation. Moreover, the compound exhibits photoconductive and pyroelectric properties and produces a very high linear electro-optical effect, owing to the very planar and layer-like solid-state packing of the compound, as deduced from the room-temperature crystal structure, determined by single-crystal X-ray diffraction (Allen *et al.*, 1988).

In light of these findings, it was deemed pertinent to study the three-dimensional structure of DCNP in greater detail, in order to try to relate more fully the structure to the physical properties observed. The investigations took the form of a 100 K neutron diffraction structural determination and variable-temperature X-ray diffraction measurements.

2. Experimental

The neutron diffraction study of monoclinic DCNP was performed on the single-crystal diffractometer, SXD, at the ISIS facility, Chilton, UK. A dichroic red/cyan crystal was mounted on a Displex closed-cycle refrigerator inside a (φ,χ) orienter and cooled to 100 K. Data were collected using the time-of-flight Laue diffraction method described by Wilson (1997). Frames of data were collected on the stationary crystal at φ and χ angles, $0 \leq \varphi \leq 90^\circ$ and $0 \leq \chi \leq 90^\circ$, in increments of 15°, up to $(\sin\theta/\lambda)_{max} = 0.7$–$0.8$ Å^{-1}. A scan time of either 700 or 800 μA h was employed for each frame (corresponding

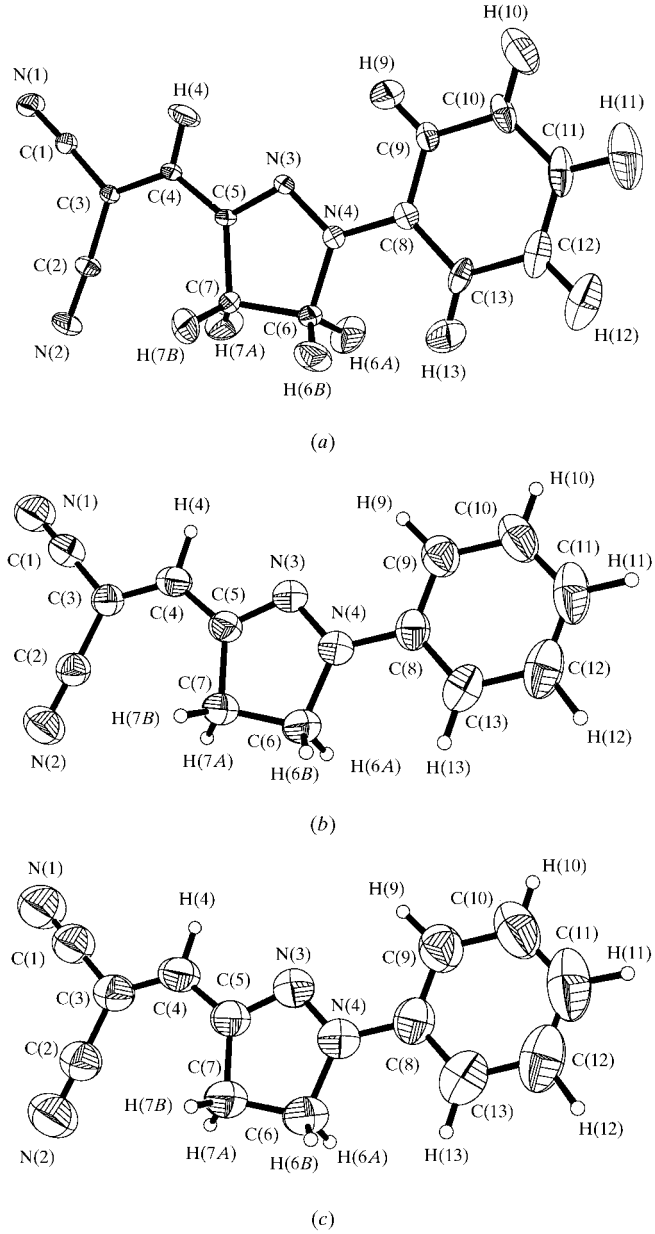

Figure 1
50% probability thermal ellipsoid plots of the (*a*) 100 K neutron structure and (*b*) 200 K and (*c*) 290 K X-ray structures of DCNP. The highly anisotropic thermal motion of the phenyl group increases smoothly with temperature in the range 90–290 K and such anisotropy is replicated entirely in the C atoms at 100 K using both X-ray and neutron diffraction. The neutron study also shows that the anisotropy in the H atoms is entirely consistent with this motion observed in the C atoms.

Table 2
Bond lengths of the 100 K neutron and 90, 100, 200 and 290 K X-ray structures of DCNP.

Bond	Distance (Å) at 100 K (neutron)	Distance (Å) at 90 K (X-ray)	Distance (Å) at 100 K (X-ray)	Distance (Å) at 200 K (X-ray)	Distance (Å) at 290 K (X-ray)
N(1)—C(1)	1.161 (3)	1.156 (3)	1.156 (1)	1.153 (3)	1.151 (4)
N(2)—C(2)	1.155 (3)	1.144 (2)	1.153 (1)	1.147 (2)	1.140 (4)
N(3)—C(5)	1.306 (3)	1.317 (3)	1.318 (1)	1.316 (3)	1.319 (4)
N(3)—N(4)	1.331 (3)	1.333 (2)	1.3319 (9)	1.332 (2)	1.324 (4)
N(4)—C(8)	1.392 (3)	1.404 (2)	1.3992 (9)	1.399 (2)	1.397 (4)
N(4)—C(6)	1.481 (4)	1.493 (3)	1.496 (1)	1.490 (3)	1.493 (4)
C(1)—C(3)	1.416 (4)	1.439 (3)	1.433 (1)	1.433 (3)	1.433 (5)
C(2)—C(3)	1.419 (4)	1.446 (3)	1.439 (1)	1.435 (3)	1.428 (5)
C(3)—C(4)	1.377 (4)	1.364 (3)	1.370 (1)	1.357 (3)	1.352 (5)
C(4)—C(5)	1.413 (4)	1.420 (3)	1.418 (1)	1.413 (3)	1.411 (5)
C(5)—C(7)	1.516 (4)	1.522 (3)	1.519 (1)	1.509 (3)	1.508 (5)
C(6)—C(7)	1.534 (4)	1.543 (3)	1.542 (1)	1.533 (3)	1.534 (5)
C(8)—C(9)	1.392 (5)	1.395 (3)	1.394 (1)	1.391 (3)	1.390 (5)
C(8)—C(13)	1.405 (4)	1.411 (3)	1.407 (1)	1.405 (3)	1.398 (5)
C(9)—C(10)	1.388 (4)	1.391 (3)	1.386 (1)	1.388 (3)	1.385 (6)
C(10)—C(11)	1.396 (6)	1.399 (4)	1.405 (2)	1.387 (4)	1.387 (8)
C(11)—C(12)	1.396 (6)	1.385 (4)	1.382 (2)	1.369 (4)	1.357 (8)
C(12)—C(13)	1.387 (5)	1.408 (4)	1.392 (1)	1.397 (4)	1.390 (7)

Table 3
C—H bond distances (Å) of the 100 K neutron structure of DCNP.

C(4)—H(4)	1.065 (7)	C(9)—H(9)	1.064 (8)
C(6)—H(6*A*)	1.093 (9)	C(10)—H(10)	1.071 (10)
C(6)—H(6*B*)	1.100 (7)	C(11)—H(11)	1.085 (8)
C(7)—H(7*A*)	1.077 (7)	C(12)—H(12)	1.084 (10)
C(7)—H(7*B*)	1.083 (9)	C(13)—H(13)	1.035 (10)

to run durations of 4–5 h per frame with the source operating at an intensity of ~170 μA h^{-1}). No variation in intensity was observed throughout, as deduced from the good merging residual factor. The reflection intensities were extracted, a semi-empirical absorption correction was applied and the data were reduced to structure factors to which a wavelength-dependent extinction correction was applied, all using standard SXD procedures (Wilson, 1997). A summary of crystal, data collection and refinement parameters is given in Table 1. Positional and anisotropic displacement parameters were refined for all atoms including the H atoms.

For the single-crystal variable-temperature X-ray diffraction studies the Siemens SMART-CCD diffractometer was ideal since, by nature of its large area, detector intensities can be recorded for a complete hemisphere of data at several different temperatures in just a few days.

The collection of the 90, 200 and 290 K data sets nominally covered over a hemisphere of reciprocal space, by a combination of three sets of exposures; each set had a different φ angle for the crystal and each frame covered 0.3° in ω. The crystal-to-detector distance was 6.004 cm. Coverage of reciprocal space was more than 97% complete to at least 25° in θ. A more extensive collection was undertaken for the 100 K data set since it was complementary to the neutron experiment. In this case, a full sphere and hemisphere of data were collected up to $2\theta = 60$ and 109°, respectively, in 0.3° steps in ω and 45 s per exposure. The resultant coverage of reciprocal space was 94% with an average redundancy of 2.4.

The same crystal was used for all four X-ray data collections and crystal decay was monitored by repeating the initial frames at the end of data collection and analysing the duplicate reflections. Isotropic extinction corrections were applied in the structural refinement from each of the conventional data collections. Positional and anisotropic displacement parameters for all non-H atoms and positional and isotropic displacement parameters were refined for all H atoms. The absolute structure could not be determined owing to the low scattering factors of the elements concerned and the wavelength of X-ray radiation used. A summary of crystal, data collection and refinement parameters is given in Table 1.

Thermal ellipsoid plots of the 100 K neutron, and 200 and 290 K X-ray structures of DCNP are shown in Figs. 1(*a*)–(*c*), respectively. The analogous plot of the 100 K X-ray structure appears to be identical to its neutron counterpart, aside from the ellipsoids of the H atoms; the plot of the 90 K X-ray structure is also similar. All non-H-containing bond lengths from each refinement are given in Table 2, whilst C—H distances determined by the neutron study are provided in Table 3.[1]

3. Discussion

3.1. The 100 K crystal structure of DCNP determined by neutron diffraction

The bond lengths (Tables 2 and 3) and angles of the crystal structure determined by neutron diffraction are significantly more accurate than the published room-temperature conventional X-ray diffraction results (Allen *et al.*, 1988). In particular, the H-atom positions are much better defined and all C—H distances are consistently longer than the reported X-ray values. From this greater accuracy, the presence of two C—H···N hydrogen bonds was indicated. No hydrogen bonding was reported in the published study. The contacts are considered to be fairly weak {C(4)—H(4)···N(1) = 2.513 (8) Å, $(x, -y, -\frac{1}{2}+z)$ [*A*]; C(12)—H(12)···N(1) = 2.49 (1) Å $(-\frac{1}{2}+x, \frac{1}{2}-y, -\frac{3}{2}+z)$ [*B*]}, but even so, they dictate the three-dimensional packing of the compound. Fig. 2 illustrates how the hydrogen bonds hold the molecules together in a corrugated layer formation. Such a parallel alignment of molecules is directly responsible for the extremely large

[1] Supplementary data for this paper, including anisotropic displacement parameters and *hkl* F_o tables, are available from the IUCr electronic archives (Reference: HA0196). Services for accessing these data are described at the back of the journal.

electro-optic coefficient reported (Miniewicz *et al.*, 1994). Hydrogen bonding thus may be considered responsible for the favourable electro-optic properties observed in DCNP. Moreover, such intermolecular interactions have also been shown to be important in other electro-optic systems (Liakatas *et al.*, 2000) and they can also strongly enhance the SHG effect (*e.g.* Sarma *et al.*, 1997). Their role in the SHG phenomenon originates from the electrostatic nature of these intermolecular interactions which provide a facile route for charge transfer between molecules. Furthermore, close proximity and good relative alignment of molecules with respect to each other promote charge transfer, and hydrogen bonding often encourages such features, as in this case. The powerful combination of this hydrogen bonding with the aforementioned high potential of the isolated molecule thus helps explain the high NLO effects observed in the bulk material.

The uncertainty in the hydrogen-bond contact distance C(12)—H(12)···N(1) is slightly greater than that for the other hydrogen bond. This is due to the markedly anisotropic thermal behaviour in the phenyl ring (see Fig. 1*a*). This thermal motion does not appear to distort the internal phenyl ring geometry [internal ring angles lie between 119.0 (3) and 121.2 (3)°]. However, the sequential increase in (*a*) the uncertainty of the C—C—H (external) phenyl angles and (*b*) their slight deviation from 120°, as one passes across the phenyl ring from C(8) towards C(11), suggests a slight geometrical distortion due to this motion. Consequently, the corresponding phenyl hydrogen fractional coordinate estimated uncertainties, particularly in the *b* and *c* directions, are noticeably large. Such deviations also appear in the geometry of the reported X-ray study (Allen *et al.*, 1988), although in that case no thermal ellipsoid plot or any discussion of thermal motion is reported. The hydrogen bonding may also cause the deviation in angles C(2)—C(3)—C(4) [124.6 (3)–125.4 (2)°], C(3)—C(4)—C(5) [127.0 (2)–128.2 (3)°] and C(4)—C(5)—C(6) [129.6 (3)–130.1 (2)°] away from the ideal 120° sp^2 geometry.

Intrigued by this atypical atomic thermal motion, we attempted to characterize it fully by performing variable-temperature single-crystal X-ray diffraction experiments.

3.2. Variable-temperature X-ray diffraction studies

In order to rule out the possibility of disorder, an incipient phase transition or some subtle form of twinning, all of which could manifest themselves in terms of anomalous thermal ellipsoids, X-ray studies of the compound were carried out at four different temperatures (90, 100, 200 and 290 K). The data collection at 100 K was the most extensive since it was complementary to the 100 K neutron study. The latter three temperatures were chosen such that the resulting anisotropic displacement parameters could be plotted against as large a temperature range as possible, within the limits of the Oxford Cryosystems Cryostream (Cosier & Glazer, 1986). Thus, the nature of the change in thermal motion with temperature could be ascertained. The 90 K temperature was chosen predominantly to investigate the possibility of a phase transition.

Simply by viewing Fig. 1, one can immediately see that the highly anisotropic thermal motion observed in the phenyl ring of the 100 K structures is present at all measured temperatures. This precludes the possibility of a phase transition in the vicinity of 100 K. Moreover, this thermal motion is seen to increase steadily with temperature, thus ruling out the possibility of any subtle twinning or static disorder. No evidence of any dynamical disorder was apparent within this temperature range either and so this was also thought to be an unlikely cause of the motion.

Having ruled out these possibilities, we tested for libration by plotting the value of each principal anisotropic displacement parameter for all non-H atoms against temperature. All plots were linear, thus indicating that the atypical motion is

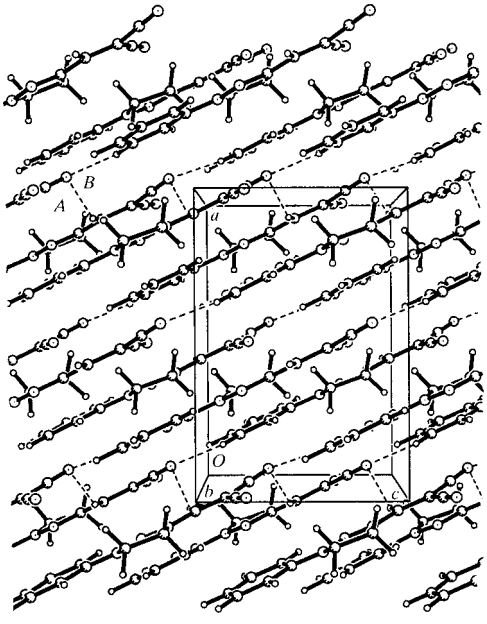

Figure 2
The molecular packing arrangement of the 100 K neutron structure of DCNP.

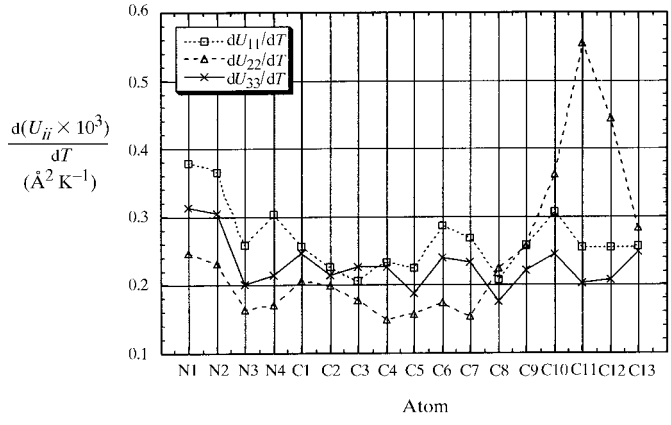

Figure 3
A graph showing the rate of increase in (*a*) U_{11}, (*b*) U_{22} and (*c*) U_{33} with temperature for each non-H atom in DCNP.

indeed due to libration. The gradient of each plot (*i.e.* the rate of increase in U_{ii} with temperature) indicates to what extent the libration is affecting each atom. Fig. 3 shows the variation in the rate of increase in each U_{ii} value with temperature across all non-H atoms. This graph reveals some interesting features: not only is libration present in the phenyl ring [C(8) → C(13)], but each nitrile group [N(1) and N(2)] is also librating to almost the same extent as the phenyl ring, and the pyrazole ring [C(5) → C(7)] is librating slightly.

Since the extent of libration does not vary in a systematic way across the molecule from the terminal atoms towards the centre, the molecule does not behave as a rigid body, librating about a pivot point. Instead, the three regions of the molecule, identified above, appear to librate in an independent but concerted way. We saw earlier that the molecules pack in a head-to-tail arrangement such that the nitrile groups in one molecule are adjacent to the phenyl groups in the next molecule. There is an aromatic C—H···N hydrogen bond [C(12)—H(12)···N(1)] between the two molecular fragments (see §3.1). Therefore, we suspect that the libration in the phenyl ring is mirrored by that in the nitrile groups because of this close proximity. The small amount of libration present in the pyrazole ring is controlled by the greater degree of libration occurring on either side of it.

3.3. Quantifying the librational effects in DCNP

In order to investigate the effects of this libration on the molecular geometry of DCNP, a series of calculations were performed, using the *THMA*11 program (Trueblood, 1990). This program is based on the methodology of Schomaker & Trueblood (1968) and Dunitz & White (1973). It performs a *TLS* correction, where elements *T*, *L* and *S* represent matrices that describe pure translational motion, pure librational motion and the correlation between the two, respectively. The structural moiety undergoing libration is treated as a rigid body librating about a specified axis, from which the mean-square torsional amplitude, $\langle\varphi^2\rangle$, is calculated. The components of *T*, *L*, *S* and $\langle\varphi^2\rangle$ are then fitted to the input atomic U_{ij} values by a linear least-squares procedure. Correlations of both overall and internal motion are deduced along with the corrections to all unique interatomic distances below a specified value. A rigid-bond analysis (Hirshfeld, 1976) is also performed, which evaluates the differences of the observed mean-square displacement amplitude (MSDA) between each atom and every other atom.

3.3.1. *THMA*11 analyses. TLS and φ analyses were carried out for the neutron and all the variable-temperature X-ray refinements. The analysis of the neutron results used all 27 atoms, whereas only 17 atoms (*i.e.* just the non-H atoms) were used in the analysis of the X-ray results. In each case, the C atoms of the phenyl ring were specified as the one librating moiety whose libration axis passes through the atom C(8) in a direction perpendicular to the plane of the phenyl ring, defined by the vector product of the bond vectors, N(3)—N(4) and C(6)—N(4). An attempt was also made to specify the nitrile groups as two further librating groups, but, in each case, this resulted in an unstable refinement presumably because the libration was not quite severe enough to be suitably accounted for by the modeling algorithms. The analyses showed that the overall libration of the phenyl group was fairly small, but increased linearly with temperature, as expected (see Fig. 4). However, the overall and internal motion correlations showed that the librational effect was rather large along the L_{33} direction [perpendicular to both the libration axis (L_{11}) and the direction of motion of the first atom of the group (L_{22}), in a right-handed system]. The translational component of the motion occurs predominantly in the principal directions, T_{11}, T_{22} and T_{33} (defined in the same axis as the librational terms). The coefficients of *S* are all zero within their estimated standard deviations. The overall amount of φ rotation and translation of the phenyl group appears to be small. However, no actual values can be assigned to this motion, since the errors calculated are as large as the values determined.

In each study, a correction was made to all bond distances which involve atoms affected by libration since libration causes an apparent *shortening* of a true interatomic distance (Cruickshank, 1956, 1961; Busing & Levy, 1957, 1964). Moreover, in the 100 K neutron analysis, a riding (Busing & Levy, 1964) and anharmonic (Ibers, 1959) correction is made for all *X*—H bond distances. The riding correction (Busing & Levy, 1964) is required since the H atoms are much lighter than any atom bonded to it (*e.g.* C or N) and so their anisotropic displacement parameters will reflect predominantly the extent of internal vibrations ensuing rather than any contribution to the molecular libration. The anharmonicity correction (Jeffrey & Ruble, 1984; Craven & Swaminathan, 1984) is required since anharmonicity exists in the *X*—H stretching vibration (Ibers, 1959), which incurs an apparent *lengthening* of the *X*—H distance. The anharmonic correction is therefore opposite to the riding correction, often resulting in a net correction of almost zero. Corrections to interatomic distances involving all libration affected non-H atoms in each analysis were insignificant (differing from the original values within one or two estimated standard deviations), whilst corrections to C—H distances made on all H atoms in the 100 K neutron

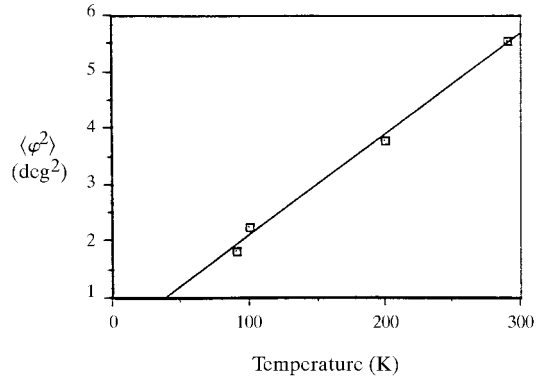

Figure 4
A plot of the overall libration amplitude of the phenyl group against temperature

Table 4
Corrections to bond distances involving H atoms from the 100 K neutron analysis.

Bond	Uncorrected distance (Å)	Anharmonic correction (Å)	Riding correction (Å)	Corrected distance (Å)
C(4)—H(4)	1.0650	−0.0114	+0.0248	1.079
C(6)—H(6*A*)	1.0931	−0.0110	+0.0314	1.113
C(6)—H(6*B*)	1.0999	−0.0035	+0.0235	1.120
C(7)—H(7*A*)	1.0769	−0.0062	+0.0318	1.102
C(7)—H(7*B*)	1.0829	−0.0113	+0.0346	1.129
C(9)—H(9)	1.0642	−0.0173	+0.0189	1.066
C(10)—H(10)	1.0708	−0.0421	+0.0314	1.060
C(11)—H(11)	1.0847	−0.0216	+0.0401	1.103
C(12)—H(12)	1.0842	−0.0152	+0.0309	1.100
C(13)—H(13)	1.0349	−0.0021	+0.0328	1.066

analysis (see Table 4) gave marked differences. In all but the 200 and 290 K X-ray analyses, corrections were made only to distances involving H atoms and atoms within the phenyl group. In the 200 and 290 K X-ray analyses, an additional correction is made to all non-H atoms. This correction is a rigid-body correction (Busing & Levy, 1964) that implies uncorrelated motion. Such motion was described in the previous section. New U_{ij} values were also calculated in order to account for the libration.[2] R factors determined for all corrected U_{ij} values ranged from 0.110 (6) to 0.276 (5), where

$$R = \left[\sum (w\Delta U)^2 / \sum (wU_{\rm obs})^2\right]^{1/2}.$$

Finally, the rigid-bond test (Hirshfeld, 1976) showed a few interesting features. In particular, ΔMSDA values for N(1) and N(2) were noticeably high in the 290 K X-ray analysis and negative trends were observed for ΔMSDA non-H − non-H values of N(2) and C(2). This means that the nitrile groups are also librating as stated previously, even though this motion could not be modelled.

3.4. Possible effects of libration on the physical properties of DCNP

Whilst the presence of libration is common in small terminal substituents such as $-CH_3$ and $-CF_3$ groups, libration of the much heavier phenyl group in a molecule is much less prevalent. As a result, a physical explanation was sought for its origin. There are no large voids in the packing arrangement in the vicinity of the phenyl group; in fact, to the contrary, hydrogen bonds couple the phenyl group to neighbouring molecules. Thus, the cause of libration in the phenyl group must be molecular in origin. The bond lengths of the phenyl group were analysed, bearing in mind that the values derived from the lower temperature measurements are necessarily more precise since the level of libration diminishes with decreasing temperature. Such bonds show a marked tendency towards quinoidal character, which is unusual in a terminal phenyl ring. Moreover, polarization of an aromatic unit into a quinoidal electronic configuration is energetically costly since the resonance stabilization of the aromatic ring must be overcome. There must, therefore, exist a source of energy that perturbs the ring current in the phenyl group and our structural analysis indicates that libration is this source. The observed tendency towards quinoidal ring character will provoke a greater ease of charge transfer within the molecule which, in turn, aids the SHG output of a material. Therefore, the libration seems to be necessary for enhancing the SHG properties of DCNP. Furthermore, the presence of libration in the nitrile groups will result in a greater susceptibility of the triple bonds to vary slightly in bond order with time. A reduction in triple bond character at time t will result in a lower bond-length alternation value (Cheng *et al.*, 1993; Gorman & Marder, 1993; Marder & Perry, 1993), which is also favourable for SHG effects.

3.5. Thermal properties of DCNP

When any NLO material is subjected to laser radiation, thermal gradients are induced within the crystal, through optical absorption. The presence of these gradients alter the phase-matching characteristics of the material since the refractive indices of a crystal vary with temperature. Therefore, it is pertinent to ascertain the thermal characteristics of such a material. In particular, specific heat, thermal expansion and thermal conductivity measurements are typically carried out to investigate the thermal behaviour (Kerkoc *et al.*, 1996). Since we were fortunate enough to have cell parameters measured at variable temperatures from the X-ray diffraction work, a thermal expansivity study on DCNP was undertaken.

The cell parameters a, b, c and β vary linearly with temperature. Fig. 5 shows the variation in the normalized cell parameters (cell length/cell length at 100 K) with temperature. The thermal expansion tensors of DCNP were evaluated by the following procedure used for monoclinic systems. The non-

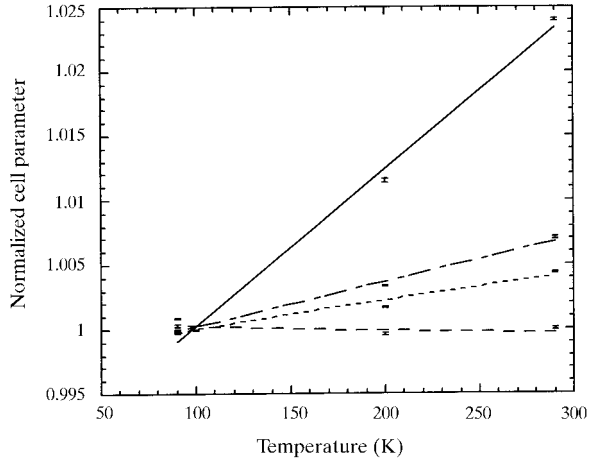

Figure 5
A plot of the normalized unit-cell parameters against temperature, $a/a_{100\ K}$ (full line), $b/b_{100\ K}$ (short and long dashes), $c/c_{100\ K}$ (dashed line) and $\beta/\beta_{100\ K}$ (dotted line).

[2] These values have been deposited with the journal (see footnote 1) and are available from the corresponding author on request, together with the uncorrected values of all anisotropic displacement parameters for each structure determination, R factors for all corrected U_{ij} values, plots of principal anisotropic displacement parameters *versus* temperature for each non-H atom, individual libration and translation tensor coefficients, overall libration amplitudes and corrected non-H containing bond distances.

Table 5
The thermal expansion coefficients and tensor elements of DCNP.

Thermal expansion coefficients ($\times 10^{-5}$ K^{-1})	
α_{11}	12.08
α_{22}	3.43
α_{33}	−0.31
α_{13}/α_{31}	−97.22
Diagonalized thermal expansion tensor elements ($\times 10^{-5}$ K^{-1})	
S_{11}	103.3
S_{22}	3.43
S_{33}	−91.53

zero thermal expansivity coefficients of the tensor are first determined by evaluating the following expressions that describe the lengths of the crystallographic axes a, b and c, and the angle β as a function of temperature. The elements of the tensor

$$\begin{matrix} \alpha_{11} & 0 & \alpha_{13} \\ 0 & \alpha_{22} & 0 \\ \alpha_{31} & 0 & \alpha_{33} \end{matrix}$$

are evaluated from

$$\alpha_{11} = \mathrm{d}[\ln(a)]/\mathrm{d}T + \cot(\beta)\mathrm{d}\beta/\mathrm{d}T$$

$$\alpha_{22} = \mathrm{d}[\ln(b)]/\mathrm{d}T$$

$$\alpha_{33} = \mathrm{d}[\ln(c)]/\mathrm{d}T$$

$$\alpha_{13} = \alpha_{31} = 1/2[\cot(\beta)\{\mathrm{d}[\ln(a)]/\mathrm{d}T - \mathrm{d}[\ln(c)]/\mathrm{d}T\} - \mathrm{d}(\beta)/\mathrm{d}t].$$

This tensor is evidently not diagonal when described in the monoclinic crystal axis frame, but can be made so by (i) using the Cartesian axes c, b and a^* (where a^* is the reciprocal space axis of a) as an orthogonal basis set and (ii) rotating the principal axis of the tensor x by an angle φ from the a^* axis in the anticlockwise sense when looking down the crystallographic b axis (right-hand side reference frame), where

$$\tan 2\varphi = 2\alpha_{13}/(\alpha_{33} - \alpha_{11}).$$

In this notation we have

$$S_{11} = \alpha_{11}\cos^2\varphi + \alpha_{33}\sin^2\varphi - \alpha_{13}\sin 2\varphi$$

$$S_{22} = \alpha_{22}$$

$$S_{33} = \alpha_{11}\sin^2\varphi + \alpha_{33}\cos^2\varphi + \alpha_{13}\sin 2\varphi,$$

where S_{ii} are the diagonal elements of the thermal expansion tensor in its principal, diagonalized form.

All values of the derivatives were taken from the gradients of relevant graphs and the reference value of β in the $\cot(\beta)$ terms was taken to be that measured at 100 K. The calculated values of both the thermal expansivity coefficients, α_{ij}, and the principal, diagonalized thermal expansion tensor elements, S_{ii}, are given in Table 5. These values are comparable to those of similar organic NLO materials (*e.g.* Bailey *et al.*, 1995; Kerkoc *et al.*, 1997).

4. Conclusions

A three-dimensional hydrogen-bonded network and some rather large anisotropic thermal behaviour has been revealed in DCNP through this structural study. The hydrogen bonding is, in part, responsible for the optimal manner in which the molecules pack for electro-optical and SHG effects. The markedly anisotropic thermal motion occurs principally in each nitrile group and the phenyl group which lie at the two extremes of the molecule. The libration is concerted since the two groups neighbour each other in a supramolecular fashion as a result of head-to-tail packing. A small amount of libration is also noted in the pyrazole ring. The libration due to the phenyl group was modelled, thus allowing a suitable correction to be applied to the molecular geometry of the phenyl group. Modified anisotropic displacement parameters for the atoms in these librating groups were also obtained. The presence of this libration appears to enhance the SHG response through its favourable perturbation of π-bonding within the ring. The variable-temperature X-ray studies were also used in order to calculate the thermal expansivity of the compound, as part of an analysis of the overall thermal behaviour of the compound.

The authors wish to thank the Institut Laue–Langevin, Grenoble, France, for financial support (JMC), the Royal Society for a Leverhulme Senior Research Fellowship (JAKH), the EPSRC for access to neutron beam-time at ISIS, Professor John Sherwood and Evelyn Shepherd for supplying the crystals and the late Professor Ken Trueblood for scientific advice.

References

Albrecht, A. C. & Morell, A. (1979). *Chem. Phys. Lett.* **64**, 46–50.
Allen, S., McLean, T. D., Gordon, P. F., Bothwell, B. D., Hursthouse, M. B. & Karaulov, S. A. (1988). *J. Appl. Phys.* **64**, 2583–2590.
Bailey, R. T., Cruickshank, F. R., Kerkoc, P., Lochran, S., Pugh, D., Sherwood, J. N., Blake, A. J. & Parsons, S. (1995). *J. Appl. Phys.* **78**, 3102–3106.
Black, S. N., Davey, R. J., Morley, P. R., Halfpenny, P., Shepherd, E. E. A. & Sherwood, J. N. (1993). *J. Mater. Chem.* **3**, 129–132.
Brédas, J. L. & Street, G. B. (1985). *Acc. Chem. Res.* **18**, 309.
Busing, W. R. & Levy, H. A. (1957). *J. Chem. Phys.* **26**, 563–568.
Busing, W. R. & Levy, H. A. (1964). *Acta Cryst.* **17**, 142–146.
Cady, W. G. (1946). *Piezoelectricity*. New York, McGraw-Hill.
Cheng, L., Gorman, C. B., Marder, S. R. & Tiemann, B. G. (1993). *Proc. SPIE*, **1775**, 19–31.
Cheng L.-T., Tam, W., Marder, S. R., Stiegman, A. E., Rikken, G. & Spangler, C. W. (1991). *J. Phys. Chem.* **95**, 10643–10652.
Cole, J. M. (1997). Ph.D. Thesis. University of Durham, England.
Cosier, J. & Glazer, A. M. (1986). *J. Appl. Cryst.* **19**, 105–107.
Craven, B. M. & Swaminathan, S. (1984). *Trans. Am. Crystallogr. Assoc.* **20**, 133–135.
Cruickshank, D. W. J. (1956). *Acta Cryst.* **9**, 757–758.

Cruickshank, D. W. J. (1961). *Acta Cryst.* **14**, 896–897.
Davydov, B. L., Derkacheva, L. D., Dunina, V. V., Koreneva, L. G., Samokhina, M. A., Zhabotinskii, M. E. & Zolin, V. F. (1970). *Zh. Eksp. Teor. Fiz. Pis'ma Red*, **12**, 24–26. [*JETP Lett.* (1970). **12**, 16–18.]
Docherty, V. J., Pugh, D. & Morley, J. O. (1985). *J. Chem. Soc. Faraday Trans. 2*, **81**, 1179–1192.
Dunitz, J. D. & White, D. N. J. (1973). *Acta Cryst.* A**29**, 93–94.
Franken, P. A. & Ward, J. F. (1963). *Rev. Mod. Phys.* **35**, 23–39.
Giordmaine, J. A. (1962). *Phys. Rev. Lett.* **8**, 19–22.
Gorman, C. B. & Marder, S. R. (1993). *Proc. Natl. Acad. Sci. USA,* **90**, 11297–11301.
Hirshfeld, F. L. (1976). *Acta Cryst.* A**34**, 909–921.
Ibers, J. A. (1959). *Acta Cryst.* **12**, 251–252.
Jeffrey, G. A. & Ruble, J. R. (1984). *Trans. Am. Crystallogr. Assoc.* **20**, 129–132.
Jen, A. K.-Y., Rao, V. P., Wong, K. Y. & Drost, K. J. (1993). *J. Chem. Soc. Chem. Commun.* pp. 90–92.
Kerkoc, P., Lochran, S., Bailey, R. T., Cruickshank, F. R., Pugh, D., Sherwood, J. N. & Blake, A. J. (1997). *J. Appl. Phys.* **81**, 624–630.
Kerkoc, P., Venkataramanan, V., Lochran, S., Bailey, R. T., Cruickshank, F. R., Pugh, D., Sherwood, J. N., Moseley, R., Goeta, A. E., Lehmann, C. W. & Howard, J. A. K. (1996). *J. Appl. Phys.* **80**, 6666–6669.
Lalama, S. J. & Garito, A. F. (1979). *Phys. Rev. A*, **20**, 1179–1194.
Liakatas, I., Cai, C., Bosch, M., Jager, M., Bosshard, C., Gunter, P., Zhang, C. & Dalton, L. R. (2000). *Appl. Phys. Lett.* **76**, 1368–1370.
Maker, P. D., Terhune, R. W., Nisenoff, M. & Savage, C. M. (1962). *Phys. Rev. Lett.* **8**, 21–22.
Marder, S. R. & Perry, J.W. (1993). *Adv. Mater.* **5**, 804–815.
Miniewicz, A., Palewska, K., Lipinski, J., Kowal, R. & Swedek, B. (1994). *Mol. Cryst. Liq. Cryst.* **253**, 41–50.
Oudar, J. L. (1977). *J. Chem. Phys.* **67**, 446–457.
Oudar, J. L. & Zyss, J. (1982). *Phys. Rev. A*, **26**, 2028–2048.
Ravi, M., Gangopadhyay, P., Rao, D. N., Cohen, S., Agranat, I. & Radhakrishnan, T. P. (1998). *Chem. Mater.* **10**, 2371–2377.
Sarma, J. A. R. P., Allen, F. H., Hoy, V. J., Howard, J. A. K., Thaimattam, R., Biradha, K. & Desiraju, G. R. (1997). *J. Chem. Soc. Chem. Commun.* pp. 101–102.
Schomaker, V. & Trueblood, K. N. (1968). *Acta Cryst.* B**24**, 63–76.
Sheldrick, G. M. (1990). *Acta Cryst.* A**46**, 467–473.
Sheldrick, G. M. (1993). *SHELXL*93. University of Göttingen, Germany.
Siemens (1995). *SMART*. Siemens Analytical X-ray Instruments Inc., Madison, Wisconsin, USA.
Trueblood, K. N. (1990). *THMA*11. University of California, Los Angeles, USA.
Wilson, C. C. (1997). *J. Mol. Struct.* **405**, 207–217.